Electronic Supplementary Information for: *A network model of transient polymers: Exploring the micromechanics of nonlinear viscoelasticity*

Robert J. Wagner, Ethan Hobbs, Franck J. Vernerey [1]
Department of Mechanical Engineering,
Program of Materials Science and Engineering,
University of Colorado, Boulder
USA

1 Boundary Conditions

1.1 A Lagrangian RVE Permits Controlled Deformation

To initially generate the extended periodic domain, the positions of the nodes, $\boldsymbol{x}^\alpha$ ($\alpha \in [1, \mathscr{N}]$) are replicated across every boundary according to:

$$\begin{aligned}
\boldsymbol{x}^T &= \boldsymbol{x}^\alpha + [+\tfrac{\partial x}{\partial y}, +h], \\
\boldsymbol{x}^B &= \boldsymbol{x}^\alpha + [-\tfrac{\partial x}{\partial y}, -h], \\
\boldsymbol{x}^R &= \boldsymbol{x}^\alpha + [+w, +\tfrac{\partial y}{\partial x}], \\
\boldsymbol{x}^L &= \boldsymbol{x}^\alpha + [-w, -\tfrac{\partial y}{\partial x}], \\
\boldsymbol{x}^{TR} &= \boldsymbol{x}^\alpha + [+w + \tfrac{\partial x}{\partial y}, +h + \tfrac{\partial y}{\partial x}], \\
\boldsymbol{x}^{TL} &= \boldsymbol{x}^\alpha + [-w + \tfrac{\partial x}{\partial y}, +h - \tfrac{\partial y}{\partial x}], \\
\boldsymbol{x}^{BR} &= \boldsymbol{x}^\alpha + [+w - \tfrac{\partial x}{\partial y}, -h + \tfrac{\partial y}{\partial x}], \\
\boldsymbol{x}^{BL} &= \boldsymbol{x}^\alpha + [-w - \tfrac{\partial x}{\partial y}, -h - \tfrac{\partial y}{\partial x}],
\end{aligned} \tag{1}$$

where superscripts T, B, R, and L denote nodes replicated to the top, bottom, left, and right of the domain, respectively. By extension, double-lettered superscripts represent the corners (*e.g.*, TR denotes the top right corner). $\partial x/\partial y$ and $\partial y/\partial x$ represent the the relative change of x at the domain bounds as a function of y, and change of y as a function of x, respectively. Note that for computational efficiency, only the nearest nodes to each boundary, defined as those less than roughly the length of a single chain (Nb) away, are replicated across their respective opposite bounds.

1.2 Eularian Conditions Prohibit Diffusion Beyond Domain Limits

To ensure that tracked nodes do not diffuse out of the simulation limits, a Eularian condition is enforced whereby any particle that exits the bounds of Ω is re-positioned into the domain according to:

$$\begin{aligned}
\boldsymbol{x}^\alpha \in \partial\Omega^T &= \boldsymbol{x}^\alpha - [\tfrac{\partial x}{\partial y}, h], \\
\boldsymbol{x}^\alpha \in \partial\Omega^B &= \boldsymbol{x}^\alpha + [\tfrac{\partial x}{\partial y}, h], \\
\boldsymbol{x}^\alpha \in \partial\Omega^R &= \boldsymbol{x}^\alpha - [w, \tfrac{\partial y}{\partial x}], \\
\boldsymbol{x}^\alpha \in \partial\Omega^L &= \boldsymbol{x}^\alpha + [w, \tfrac{\partial y}{\partial x}],
\end{aligned} \tag{2}$$

[1] correspondence to: franck.vernerey@colorado.edu

where $\boldsymbol{x}^{\alpha} \in \partial\Omega$ denotes that node α has moved into the T, B, R, or L periodic boundaries of the domain, Ω, respectively. Once nodes are repositioned in Ω, they are replicated at each time step according to the conditions of ESI Section 1.1.

2 Domain Size Convergence

In order to select an appropriate initial square domain size (for which $h = w$), the networks' global stress responses is examined. The smallest domain dimension (*i.e.*, w at full deformation) must be larger than the contour length of a single chain ($Nb = 3.5\zeta$). To enforce this, the minimum domain size considered in this work contains $\mathscr{N} = 225$ nodes, which corresponded to initial domain dimensions of $11.25 \times 11.25\zeta$ and final dimensions of $5.625 \times 22.5\zeta$ (after 100 % incompressible, uniaxial network stretch is applied), which satisfies the condition $w > Nb$. The ensemble averaged stress response of 10 trial networks, containing $\mathscr{N} = 225$, $\mathscr{N} = 400$, and $\mathscr{N} = 625$ nodes (which correspond to roughly 15, 20 and 25 nodes per edge, respectively) is displayed in Fig. S1. Notably, there is no significant change in the measured stress response as the domain size is increased from 225 nodes to 625 nodes, and so the domain size was set to $\mathscr{N} = 225$ for computational efficiency.

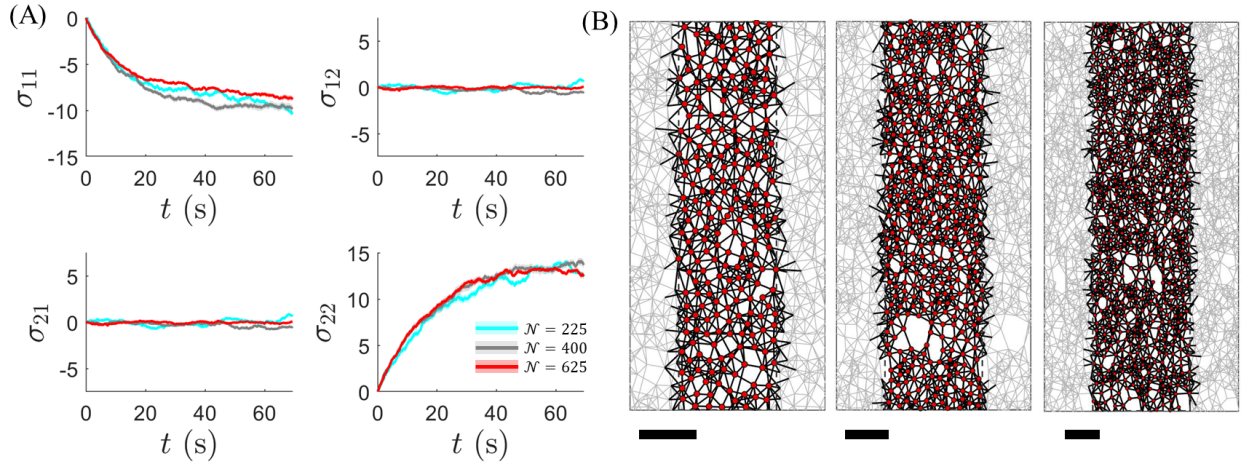

Figure S1: **(A)**The four components of virial stress, ensemble averaged over 10 distinct trials (each), are plotted for increasing domain sizes, $\mathscr{N} = 225$ nodes (blue), $\mathscr{N} = 400$ nodes (grey), and $\mathscr{N} = 625$ nodes (red). **(B)** Networks at $\epsilon \approx 1$ are plotted from left to right for $\mathscr{N} = 225$ nodes, $\mathscr{N} = 400$ nodes, and $\mathscr{N} = 625$ nodes, respectively. Scale bars under each snapshot represent the contour length of a single chain, Nb (or 3.5ζ).

3 Time Step Convergence

In order to select an appropriate time step size, Δt, the networks' stress responses, mean bond kinetic rates, and degree of homogenization were considered. The time step was initially set such that it was two orders of magnitude lower than the inverse of the stress-free bond detachment rate, $k_d^0{-}1 = 100$ s, or the highest strain rate investigated, $\dot{\varepsilon}^{-1} = 50$ s. As such, the largest time step considered was $\Delta t = 0.5$ s. As depicted in Fig. S2, decreasing Δt over $\Delta t = [0.5, 0.1, 0.05, 0.01]$ s, did not influence the measured stress response of the networks (Fig. S2.A). Nor did it impact the average measured bond kinetic rates and - by extension - the average coordination number of the network (Fig. S2.B). In the scope of this work, Δt was conservatively set to 0.1% of the highest inverse strain rate or $\Delta t = 0.05$ s, which is well below the convergence threshold while also allowing for relatively low computational time.

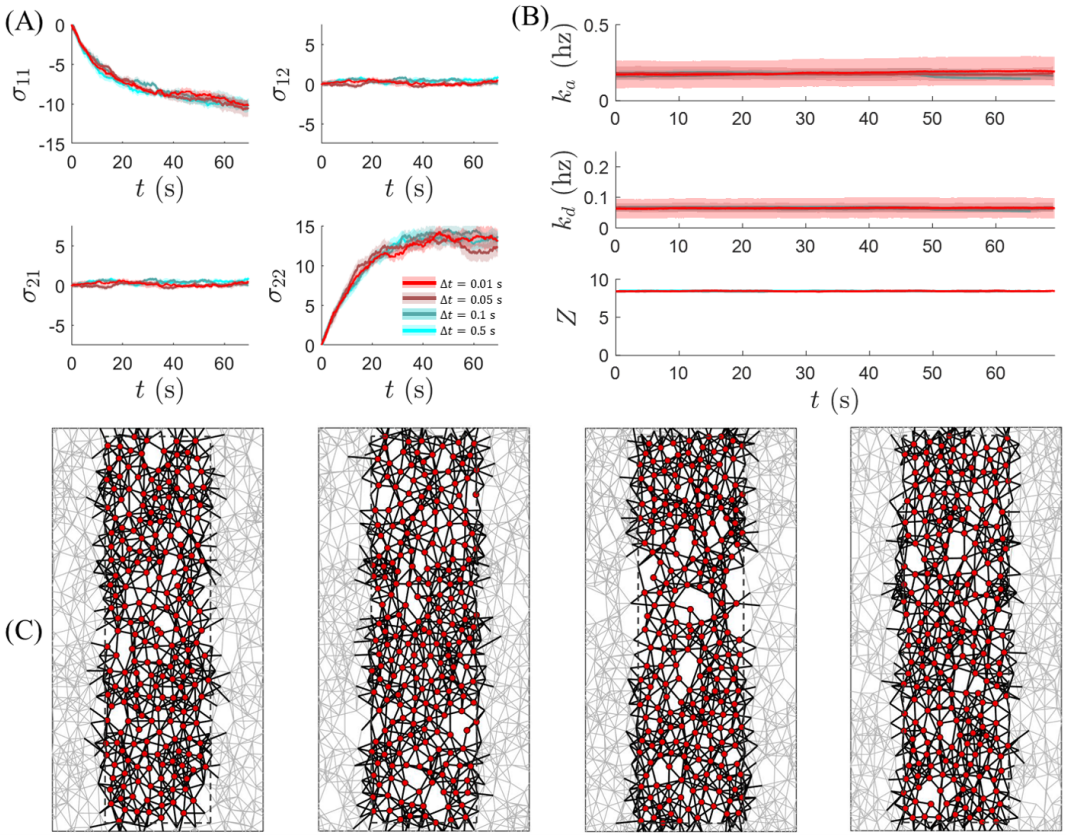

Figure S2: **(A)** The four components of virial stress are plotted for decreasing timesteps, $\Delta t = 0.5$ s (blue), $\Delta t = 0.1$ s, $\Delta t = 0.05$ s, $\Delta t = 0.01$ s (red). **(B)** The attachment (top) and detachment (center) rates are plotted with respect to time for the four respective time steps, along with the resulting average coordination number (bottom). **(C)** Networks at $\epsilon \approx 0.9$ are plotted from left to right for $\Delta t = 0.5$ s, $\Delta t = 0.1$ s, $\Delta t = 0.05$ s, $\Delta t = 0.01$ s, respectively.

4 Stress Response of a Network with Gaussian Springs

As a benchmark comparison between the discrete framework and continuum approach, networks of Gaussian springs were modeled and deformed according to the load history of Fig. 6.A in the manuscript. Force-dependent detachment through Eyring's model was maintained in order to ensure that the networks achieved initial steady state and observed detailed balance. The normal stress response (ensemble averaged for fifty networks, each) during loading and relaxation is depicted in Fig. S3.A and B, respectively, for five different strain rates. As expected, the stress predicted by the discrete and continuum models are in good agreement during loading when Guassian chains are used in both frameworks. However, since force-dependent bond dynamics were maintained, a non-exponential decay in stress is still observed during relaxation.

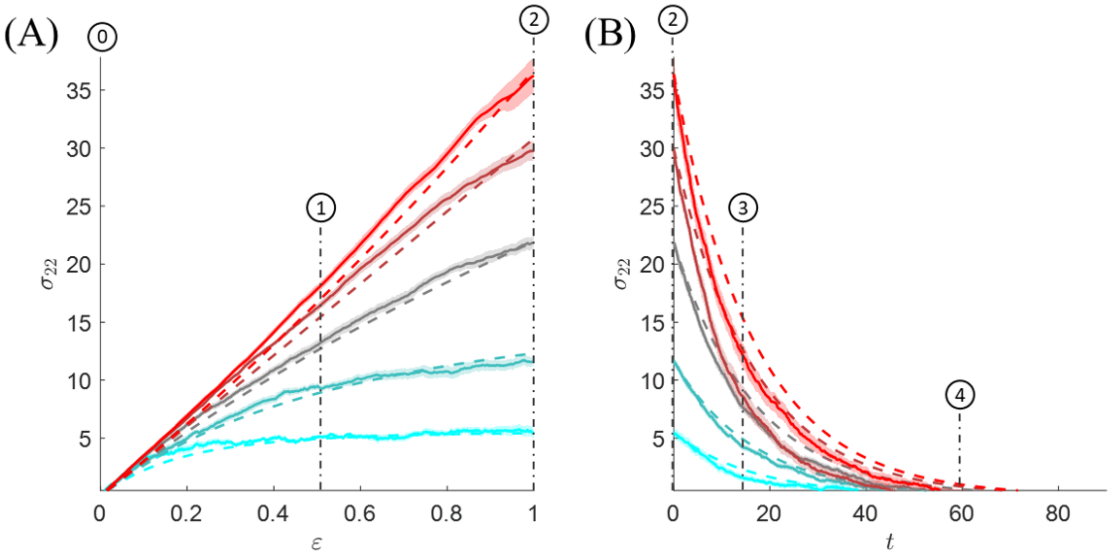

Figure S3: **(A)** Normal stresses from creep experiments are plotted with respect to engineering strain, $\epsilon = F_{22} - 1$, for $W \approx 1/8$ (cyan), $W \approx 1/4$ (teal), $W \approx 1/2$ (grey), $W \approx 1$ (maroon), and $W \approx 2$ (red). **(B)** Normal stresses from relaxation experiments are plotted with respect to time for three different initial values of stress. All results from the discrete model are plotted as continuous curves with standard error represented by the shaded region, and results from TNT are plotted as dotted curves.